Volume 1 | Number 1 | Jan 2013 | Pages 1–100

Journal of
Materials Chemistry A

Materials for energy and sustainability
www.rsc.org/materialsA

Li⁺

ROYAL SOCIETY
OF CHEMISTRY

ROYAL SOCIETY
OF CHEMISTRY

www.rsc.org/materialsA

Improved electrochemical performance of $Na_3V_2(PO_4)_3$ cathode by B-doping of carbon coating layer for sodium-ion batteries

Wei Shen[a], Hui Li[d], Cong Wang[a], Zhihong Li[b], Qunjie Xu[b], Haimei Liu[a,b*], Yonggang Wang[c]*

[a]State Key Laboratory of Chemical Resource Engineering, Beijing University of

Chemical Technology, Beijing 100029, China

[b]Shanghai Key Laboratory of Materials Protection and Advanced Materials in Electric

Power, Shanghai University of Electric Power, Shanghai 200090, China

[c]Department of Chemistry and Shanghai Key Laboratory of Molecular Catalysis and

Innovative Materials, Fudan University, Shanghai 200433, China.

[d]Beijing Key Laboratory of Environmental Science and Engineering, Beijing Institute

of Technology, Beijing 100081, China.

---

* The authors to whom correspondence should be addressed, e-mail: liuhm@shiep.edu.cn (H. Liu), ygwang@fudan.edu.cn (Y. Wang)

Abstract: Boron-doped carbon coating is initially used to improve the electrochemical performance of $Na_3V_2(PO_4)_3$ cathode materials of sodium-ion batteries. Based on the precise analysis of Raman spectroscopy, electrochemical impedance spectroscopy and X-ray photoemission spectroscopy, it is found that there are four different B-doping species (B_4C, BC_3, BC_2O and BCO_2) in various Boron-doped carbon coated $Na_3V_2(PO_4)_3$ samples; moreover, different B-doping species in the carbon coated layer have different impacts on the improvement of the electrochemical performance of $Na_3V_2(PO_4)_3$. Compared to lithium-ion batteries, the mechanism of B-doped carbon coating on the improvement of the electrochemical performance in sodium-ion batteries are different. Due to the introduction of O atom in the carbon coated layer, BC_2O and BCO_2 significantly increase numerous extrinsic defects and active sites, which could significantly accelerate Na^+ transport in the carbon layer. Therefore, it is unexpectedly demonstrated that the $Na_3V_2(PO_4)_3/C+B$, in which with the largest total amounts of $BC_2O + BCO_2$, exhibits the best electrochemical performance, particularly the high-rate performance and cycling stability, as an example, when the discharging rate increased from 0.2 C to 5 C, it delivers 95.8 mAh g^{-1} to 90.3 mAh g^{-1} and an amazing capacity retention of 94% is achieved.

Introduction

It is undeniable that the world has to face energy management issues in recent years,[1] for this reason, and taking into consideration recent concerns about a possible

lithium shortage with the spread of electronic devices and electric vehicles, it is highly desired to develop alternative energy storage systems that could complement the existing lithium-ion batteries (LIBs). For this purpose, sodium-ion batteries (SIBs) may be a suitable choice depending on battery cost, safety and raw material abundance. Therefore, in order to get more economic, safer, high energy density and long life batteries, it is of the greatest importance to search for and optimize new electrode materials for cathodes and anodes.[2]

Recently, active phosphates with NASICON structure, particularly sodium vanadium phosphate ($Na_3V_2(PO_4)_3$), have larger reversible gravimetric energy density (400 Wh/kg^{-1}, 117.6 mAh g^{-1} × 3.4 V for the V^{3+}/V^{4+} redox couple) than other related compounds, such as $NaCoO_2$, $NaNiO_2$ and $Na_3Fe_2(PO_4)_3$.[3,4] Moreover, during the charge/discharge process, the large sodium ions (ionic radius 1.02 Å)[5] can be easily inserted into/extracted from $Na_3V_2(PO_4)_3$ because it possesses a large sodium site based on a 3D framework, as shown in Scheme 1. In this structure, the $V_2(PO_4)_3$ scaffold is built of each VO_6 octahedron links via corners sharing with three PO_4 tetrahedrons, whereas Na^+ are occupied two different sites. At low Na^+ content (x < 1 in $Na_xV_2(PO_4)_3$) an octahedral site, Na1, is selectively occupied. With x > 1, the Na^+ are randomly distributed among the Na1 and three 8-coordinate sites, Na2. Moreover, both Na1 and Na2 are accommodated in large tunnels of different plane. Therefore, the open 3D nature of the structure allows easy migration of the Na^+ between Na1 and Na2.[2] The theoretical discharge capacity of $Na_3V_2(PO_4)_3$ varies between 117.6 and

236 mAh g^{-1} depending on the voltage range and the variation between V^{3+}/V^{4+} and V^{2+}/V^{3+} redox states, corresponding to the voltage plateaus at 3.4 V and 1.6 V vs. Na$^+$/Na, respectively.[6,7] However, the unfavorable electronic conductivity of phosphate framework restricts the high rate operation and cycling stability of Na$_3$V$_2$(PO$_4$)$_3$, which is similar to LiFePO$_4$, Li$_3$V$_2$(PO$_4$)$_3$ and Li$_2$FeSiO$_4$.[8-10] Therefore, a new strategy is required to realize ultra-high power Na$_3$V$_2$(PO$_4$)$_3$ by enhancing its electronic conductivity.

One of the low cost and high-efficiency ways to improve the electronic conductivity of NASICON-structured cathode materials is to coat the conductive carbon layers on the surfaces of these materials.[11-15] Compared with other kinds of surface coating approaches, carbon coating has many advantages: (1) the carbon coated layer can effectively enhance the electronic conductivity of electrode materials; (2) it can uniformly adhere to the surface of electrode materials, thus restricting the growth of particle of electrode materials; (3) it can also avoid the electrode materials direct contact with the electrolyte, thereby avoiding occurrence of side reaction.[16,17] As a result, the electrochemical performance of the electrode materials will be obviously improved. Therefore, how to improve the electronic conductivity of carbon layer is highly desirable. At present, non-metallic elements doping which include nitrogen, boron and sulfur doping are widely used in carbon coated electrode materials in LIBs[9,18-22] or pure carbon-based materials[23,24] and exhibits excellent modification effects. In our previous work, a cathode material Li$_3$V$_2$(PO$_4$)$_3$ of LIBs

was modified by boron-doped carbon coating, and demonstrated that the graphite-like BC_3 dopant species played a huge role on improving the electronic conductivity and electrochemical activity.[9] However, for SIBs, the related works are rarely reported, and moreover, whether the mechanism of boron-doing in SIBs is similar with the one in LIBs, and whether boron-doing in SIBs can also improve the electrochemical performance of electrode material as good as in LIBs, these are not having been systematically investigated and analyzed so far.

In this work, we firstly adopt boron doped carbon coating approach to modify the electrode materials of SIBs and explain in detail the causes of the modification effects. As a result, compared with the bare carbon coated $Na_3V_2(PO_4)_3$, boron-doped carbon coated $Na_3V_2(PO_4)_3$ composite exhibits a remarkable improvement in Na storage performance, especially its rate capability and cycling performance. Moreover, the relationship between the electrochemical performance of various boron-doped carbon coated samples and the doping species in carbon layer was analyzed and explained in detail in SIBs and LIBs.

Experimental Section

Materials preparation

Various kinds of NVP-C-B materials and NVP-C materials were synthesized by using of a sol-gel method, and NaOH, V_2O_5, H_3PO_4, citric acid and sodium tetraphenylborate ($NaBC_{24}H_{20}$) were used as raw materials. Citric acid and $NaBC_{24}H_{20}$ were used as carbon source and boron source, respectively. To synthesize the

NVP-C-B materials, citric acid and $NaBC_{24}H_{20}$ were dissolved in distilled water with continuous stirring at 80 ℃ and after being dissolved completely, NaOH, V_2O_5 and H_3PO_4 (85%wt.) in stoichiometric amounts were added into the above solution in turn under constant stirring. Meanwhile, the solution was continuously stirred and heated at 80 ℃ to form a uniform solution. The mixture was heated for several hours to evaporate the water until a green gel was generated from sol. After the transformation, the gel precursors were dried in an vacuum oven at 80 ℃ for at least 8 hours. The obtained powers were ground and pre-heated at 300 ℃ in nitrogen atmosphere for 4 h. Then, the powders were ground again and sintered at 850 ℃ in a nitrogen atmosphere for 8 h to obtain the final NVP-C-B material. To prepare the samples with different boron content, NVP-C-B with various molar ratios of B to C with 0.45 %, 0.75 % and 0.105 % were prepared and marked as NVP-C-B0.45%, NVP-C-B0.75% and NVP-C-B0.105%, respectively. For comparison, a controlled NVP-C sample was also prepared, and the synthetic method was the same as above-mentioned except for the addition of $NaBC_{24}H_{20}$.

Characterizations

Powder X-ray diffraction patterns of various NVP-C-B and NVP-C samples were performed at a scanning rate of 5 min^{-1} in the 2θ range from 10 to 60° by using the D/max-Ultima III Diffractometer at 40 kV, 40 mA with Cu-Kα radiation (λ = 0.154 nm). The morphology and microstructure of the samples were characterized by using scanning electron microscopy (FE-SEM, Zeiss Supra 55) and energy-dispersive X-ray

spectroscopy (EDX). The HRTEM images were obtained using a high-resolution transmission electron microscope (Hitachi H-800). The structural property of NVP-C and various NVP-C-B samples were achieved on a labRAM ARAMIS laser Raman spectroscopy equipped with a 532 nm Ar-ion laser. The carbon content of the different samples were measured using organic element analyzer (Thermo Scientific, Flash 2000 series). The XPS spectra were performed at room temperature on a PHI Quantera SXM scanning X-ray microprobe with a 100 mm beam size, using an Al Ka (l = 0.83 nm, hn = 1486.7 eV) X-ray source operated at 2 kV and 20 mA.

Electrochemical measurement

Electrochemical performances of the NVP-C and various NVP-C-B samples were performed using 2032-type coin half-cells and using Na metal foil as the counter electrode. The work electrodes consisted of 80 wt.% of active material, 10 wt.% of carbon black, and 10 wt.% of a polyvinylidene difluoride (PVDF) dissolved in *N*-methylpyrrolidone as the binder. Then the slurry was spread onto aluminum foil and the electrodes were dried at 100 °C in vacuum for at least 10 h. The half cells were assembled in an Ar-filled glove box. The active material load in each coin cell was typically 2.0-2.5 mg cm^{-2}. The electrolyte was 0.8 M NaClO$_4$ in ethyl carbonate (EC) and diethyl carbonate (DEC) with the volumetric ratio of 1 : 1, and a polypropylene micro-porous film (Cell-gard 2300) was used as the separator. The assembled cells were cycled at different charge/discharge rates on a LAND CT2001A test system (Wuhan, China) at room temperature in the potential range of 2.7-4.0V

(versus Na^+/Na). Before the charge/discharge measurements, the cells were pre-cycled three times. Electrochemical impedance spectroscopy (EIS) tests and cyclic voltammetry (CV) measurements were obtained on a CHI650D (Chenhua, Shanghai) electrochemical workstation.

Results and discussion

To confirm the effects of boron-doped carbon coating on the structure of $Na_3V_2(PO_4)_3$, XRD observations of the NVP-C and various NVP-C-B were tested and displayed in Fig. S1†. It is obvious that there is nearly no difference between NVP-C and various NVP-C-B samples, all the reflections could be well indexed to the R3-c space group and in good agreement with the framework of a rhombohedra NASICON structure, including the peak positions and intensities.[25-27]. Moreover, Rietveld refinements were also conducted for all the NVP samples (Fig. S2†). In this work, the refinements were carried out using the GSAS program suite. The data of calculated lattice parameters are listed in Tables S1†. It is demonstrated that the value of the a axis (a = b axis), c axis and the lattice volume are nearly no obvious difference for various $Na_3V_2(PO_4)_3$ samples, indicating B was not doped into $Na_3V_2(PO_4)_3$ structure and not affect its crystal structure. Besides, two relatively strong peaks (104) and (113) were selected and the ratios of $I_{(104)}/I_{(113)}$ for various $Na_3V_2(PO_4)_3$ samples were calculated. The $I_{(104)}/I_{(113)}$ for NVP-C, NVP-C-B0.24%, NVP-C-B0.38% and NVP-C-B0.51% are 0.6482, 0.6391, 0.6466 and 0.6522, respectively. It is noticed that the $I_{(104)}/I_{(113)}$ of NVP-C and various NVP-C-B samples are very close to each other, that is also to say

boron-doped carbon coating does not affect the crystal structure of the $Na_3V_2(PO_4)_3$.

As shown in Fig. 1 and Supporting Information Fig. S3†, morphology and size of

NVP-C and various NVP-C-B samples after annealing at 850 ^{o}C were further

investigated by scanning electron microscopy (SEM). SEM images show that all the

NVP-C and NVP-C-B samples have an irregular morphology and the average particle

size are all about 1 to 2 μm. In other word, there is no difference on morphology

between NVP-C and NVP-C-B. In order to confirm the composition and distribution

of boron in the surface carbon coated layer, EDX mapping analysis was also carried

out. Based on the EDX mapping images of B, C, Na, V and P elements in Fig. 1, it

can be clearly observed that boron is successfully doped and the B-doped carbon

coated layer was completely and uniformly distributed on the surface of $Na_3V_2(PO_4)_3$

particles, which is expected to provide facile electronic transport for the electrons in

the charge/discharge process.

    The detailed morphology and microstructure of the synthesized NVP-C and

NVP-C-B0.38% were further explored by HRTEM, as shown in Fig. 2. It is

noticeable that a homogeneous and uniform graphite-like amorphous carbon layer is

formed on NVP-C and NVP-C-B0.38% surface, and the thickness is around 5 nm.

Furthermore, the carbon contents of various $Na_3V_2(PO_4)_3$ composites in this report

have been measured by the organic element analyzer. The carbon contents of NVP-C,

NVP-C-B0.24%, NVP-C-B0.38% and NVP-C-B0.51% are about 8.60, 7.54, 6.43 and

5.44%, respectively. The HRTEM images and the selected area electron diffraction

(SAED) patterns in inset in Fig. 2b and d indicate the high crystallization character of both samples, and the marked lattice fringes with d-spacing of 0.251 and 0.373 nm corresponding to the (300) and (113) planes of the NASICON-type $Na_3V_2(PO_4)_3$.

In order to further observe the effects of B-doping on the defect level of various $Na_3V_2(PO_4)_3$ surface carbon layer, Raman spectra of NVP-C and various NVP-C-B samples are tested. It is obviously demonstrated in Fig. S4† that the Raman spectra of all samples show two conspicuous peaks of the disorder-induced phonon mode (D-band), graphite band (G-band) and a very weak 2D-band. Generally, the value of the intensity ratio of D-band to G-band (I_D/I_G) is used to estimate the degree of disorder and defects of carbon materials.[28,29] The values of I_D/I_G for NVP-C, NVP-C-B0.24%, NVP-C-B0.38% and NVP-C-B0.51% are around 0.96, 1.02, 1.04 and 1.01, respectively. Obviously, the value of I_D/I_G of all NVP-C-B samples are larger than that of NVP-C sample, indicating that more defects sites existed in the carbon coated layers in various NVP-C-B than in NVP-C, which is caused by the heterogeneous boron doping. However, it is noteworthy that the I_D/I_G ratio of NVP-C-B0.38% is the highest in all four samples, indicating most defects sites are existed in NVP-C-B0.38% surface carbon coated layer. It is well-known that the ionic radius of Na^+ (1.02 Å) is much larger than Li^+ (0.76 Å) and the equivalent weight of Na is also higher than Li; therefore, compared with Li^+ diffusion, Na^+ diffusion across the interface between the electrolyte and electrode becomes more kinetically logy. Therefore, it is quite reasonable to imagine that the large amount of topological

defects sites produced by the boron doping, especially for the NVP-C-B0.38% sample, can be beneficial to Na^+ pass through and storage and thus further improve the electrochemical performance of NVP-C-B cathode materials.

In order to clarify the electrochemical intercalation behavior of Na ion, cyclic voltammetry for NVP-C and various NVP-C-B samples was performed in the potential window of 2.7-4.0 V at 0.09 mV/s, as shown in Fig. S5†. One couple of oxidation and the corresponding reduction peaks near 3.4 V can be observed, which are typical of Na-ion extraction and insertion with the V^{4+}/V^{3+} redox couple. Obviously, all the oxidation peaks for various $Na_3V_2(PO_4)_3$ samples are almost located at 3.5 V; however, the potential of corresponding reduction peak for NVP-C is lower than those for all NVP-C-B samples, indicating that the larger polarization for NVP-C. Due to the slow scanning rate of 0.09 mV/s, the oxidation and the corresponding reduction peaks for various NVP-C-B samples are nearly no difference. Moreover, the CV for NVP-C-B0.38% was also performed in the potential window of 2.7-4.0 V with different scanning rates of 0.05, 0.07 and 0.09 mV/s, as exhibited in Fig. 3a. The oxidation peaks located at 3.457, 3.461 and 3.462 V, and corresponding reduction peaks are 3.254, 3.224 and 3.203 V at different scanning rates, respectively. The sharp peaks suggest the good reversibility of phase transformation from $Na_3V_2(PO_4)_3$ to $NaV_2(PO_4)_3$. The inset in Fig. 3a depicts the unit cell structures of typical two-phase reaction causing the change from the $Na_3V_2(PO_4)_3$ to the $NaV_2(PO_4)_3$ phase.[30] In order to investigate the rate capability of NVP-C and various NVP-C-B electrodes at

different C-rates, an rate capability test from 0.2 to 5 C (where 1C corresponds to the complete discharge in 1h, 1 C = 117.6 mA g^{-1}) is conducted and shown in Fig. 3b). It is obvious that all NVP-C-B samples show much better rate capability than NVP-C; moreover, the doping content of boron in the carbon coated layer has an important impact on the electrochemical performances of NVP-C-B. Among the various NVP-C-B samples, NVP-C-B0.38% shows the best rate capability, followed by NVP-C-B0.24% and NVP-C-B0.51%. It must be point out that the variation tendency of electrochemical performance of various $Na_3V_2(PO_4)_3$ samples shows an unexcepted consistence with the variation of the intensity ratios of I_D/I_G in Raman spectra (Fig. S4†). That means the more extrinsic defects sites existed in the carbon coated layer, the better improvement of electrochemical performance of NVP-C-B electrodes. Fig. 3c shows a comparison of rate capability of the NVP-C and NVP-C-B electrodes from 0.2 C to 5 C. The NVP-C-B0.38% electrode with the best electrochemical performance could deliver high discharge capacities of 95.8 and 95.2 mAh g^{-1} at low rates of 0.2 and 0.5 C, respectively, which further demonstrates an excellent rate capability with a value of 93.1 at 1 C, 93.0 at 2 C, 93.0 at 3 C and 90.3 mAh g^{-1} at 5 C. When recycled at 3, 0.5 and 0.2 C, its discharge capacity can still reach 93.4, 93.8 and 93.9 mAh g^{-1}, respectively. Compared with the initial rates, there is almost no specific capacity loss when recycled to the initial rates. Moreover, the discharge curves of NVP-C-B0.38% at various C-rates are further studied to confirm the excellent rate capability. It is apparent that the platform specific capacity of NVP-C-B0.38%

between small current densities and high current densities are almost similar as shown in Fig. 3d, and the potential polarization from 0.2, 0.5, 1, 2, 3 to 5 C are 0.09, 0.15, 0.18, 0.24, 0.28 and 0.36 V, respectively (inset in Fig. 3d). The rate performances of NVP-C-B cathode are clearly superior to most of recently reported $Na_3V_2(PO_4)_3/C$ cathode materials prepared by solid-state and solution reaction routes.[7,30] For instance, A $Na_3V_2(PO_4)_3/C$ cathode was synthesized by means of a polyol-assisted pyrosynthetic reaction, and its specific discharge capacities at 1.33 and 2.67 C were 88 and 65 mAh g^{-1}. Moreover, when the rate was increased to 5.33 C, the capacity was only approximately 25 mAh g^{-1}.[7] Another $Na_3V_2(PO_4)_3/C$ electrode with a novel one-dimensional (1D) nanostructure was prepared by electrospinning method, and its specific discharge capacities at 2 and 5 C were only 77 and 58 mAh g^{-1}.[30]

Furthermore, the cycle performance of NVP-C and NVP-C-B electrodes were further investigated at different discharge C-rates of 0.2, 1, 5 and 10 C, as shown in Fig. 4. It should be noted that in order to optimize the discharge capacity of various electrodes, a small charge C-rates of 0.2 C is employed. Obviously, all NVP-C-B electrodes exhibit much better electrochemical performances than NVP-C; moreover, the NVP-C-B0.38% also exhibits the best stable long-term cycle stability at different discharge C-rates. When cycled at small C-rates of 0.2 C and 1 C, the difference of the electrochemical performance between NVP-C and NVP-C-B electrodes is small; however, when cycled at high C-rates of 5 C and 10 C, the discharge specific capacity and cycle stability of NVP-C are far less than NVP-C-B electrodes. When the

NVP-C-B0.38% is cycled at 5 C (Fig. 4c), its initial capacity could reach up to 95.4

mAh g^{-1}, after 50 cycles, its specific capacity is still 76.6 mAh g^{-1} , which is much

higher than the NVP-C with 78.2 mAh g^{-1} at first cycle, and 13.0 mAh g^{-1} at 50th

cycles. Even at higher C-rates of 10 C (Fig. 4d), the NVP-C-B0.38% also exhibits the

best rate capability and cycle stability, its discharge specific capacity exhibits better

retention from an initial value of 87.1 mAh g^{-1}, finally stabilized at 70.5 mAh g^{-1} at 50

cycles. In addition, the coulombic efficiency (calculated from the discharge/charge

capacity) can reach up to approximately 100% in the overall battery operation,

demonstrating a prominent high-rate cycling performance of NVP-C-B0.38%

electrode.

Meanwhile, the cycle stability of NVP-C-B0.38% under 0.2 C and 10 C was

further explored and presented in Fig. S6†. Fig. S6a† shows the typical initial

charge/discharge profiles of NVP-C-B0.38% in the potential range of 2.7-4.0 V vs.

Na$^+$/Na at 0.2 C, the initial specific capacity is 98.3 mA g^{-1}, after 40 cycles, its

specific capacity is still 96.6 mAh g^{-1}; moreover, the charge/discharge profiles nearly

no apparent change in the cycling test, including potential platform and discharge

specific capacity. Furthermore, the obvious charge/discharge plateau is observed at

3.42/3.33 V at the first cycle, with only a little potential polarization (0.09V) during

the charge/discharge process. Even at higher current density of 10 C (Fig. S6b†), the

NVP-C-B0.38% also exhibits the high-rate capability and stable long-term cycle

stability; however, it must be pointed that under such a large discharge current density

of 10 C, the potential polarization obviously increases to 0.48 V.

In order to carefully analyze the chemical bonding between carbon and boron in the carbon-coated layer, X-ray photoemission spectroscopy (XPS) studies were examined. Moreover, based on the atom percents (At%) of carbon and boron in XPS data as well as the carbon contents of various NVP-C-B samples, the B-doping ratio in various NVP-C-B has been calculated, and the actual percentage composition of boron in NVP-C-B0.24%, NVP-C-B0.38% and NVP-C-B0.51% are 0.578%, 0.709% and 0.837%, respectively. Based on the C1s spectrum of NVP-C (Fig. 5a), the peak at binding energy of 284.6 eV belongs to the sp^2 graphite C=C bond. The other peaks at higher energy can be attributed to the sp^3 carbon with some different C-O bonding configurations. These C-O bonding configurations contain the C-O bond at 285.8 eV, C=O bond at 287.8 eV and O=C-O bond at 289.3 eV.[31] However, after boron doped in the carbon layer, an obvious new peak located at ~283.6 eV,[32,33] which can be ascribed to the C-B species, is clearly appeared in C1s spectra for all NVP-C-B samples as shown in Fig. 5b-d. Moreover, with the gradual increase of the B content, the peak area of the C-B species exhibits the similar increase tendency; thus demonstrating the boron have been successfully doped into the interior carbon coated layer on different NVP-C-B samples. Besides, intensity of the peak ascribed to the C-O bond increases to a much higher value after boron doped in the carbon layer. The reason of the increase of C-O bond could be explained combined with the O1s spectra (Fig. S7†). In O1s spectrum of NVP-C (Fig. S7a†), the peak at around 532.0 eV

corresponds to the C=O bond.[9] After boron doped in the carbon layer, the aera of this peak obviously increases because of the appearance of new B-O bond. Therefore, based on the appearance of new B-O bond, a large number of O enter into the interior carbon layer, resulting into the increase of C-O bond in Fig. 5b-d. These results, once again, certify that the boron have been successfully doped into interior carbon layer on the NVP-C-B surface. Due to the boron-doping within a certain doping ratio can efficiently increase the electronic conductivity of the carbon coated layer on the electrode material, it is easy to understand that the electrochemical performance of different NVP-C-B samples are much better than that of the bare NVP-C.

Now, in order to clarify why NVP-C-B0.38% exhibits the optimal performance in all doped samples, boron-doping species and accurate contents of boron presented in various NVP-C-B were proved by XPS as depicted in Fig. 6. The XPS results of B1s for various NVP-C-B are carefully analyzed and compared with each other. As is shown in Fig. 6a, c and e, the B1s spectra of various NVP-C-B samples are all divided into four main contributions: the peak at the lowest binding energy ~187.9 eV belongs to B_4C type bond,[34] the peak at ~190.1 eV is assigned to BC_3 type bond[34,35] and the peaks at ~191.1 eV and ~192.2 eV are correspond to the BC_2O and BCO_2 type bonds, respectively. It can be clearly seen that for all NVP-C-B samples, the distribution and contents of various B-C bond types are different. Therefore, according to the above analysis of the XPS, the idealized schematic structures for the surface carbon layer of B-doping are depicted in Fig. 7a. As shown in Fig. 6b, d and f, compared with other

three B types (BC_3, BC_2O and BCO_2), the peak intensity of the B_4C doped type in various NVP-C-B samples are all relatively low and this B_4C type bond is accompanied by defects inside the carbon layer.[36] Therefore, taking into account the low content of B_4C doped type (below 4%), this doped type makes relatively little impact on the improvement of electrochemical performance of various NVP-C-B samples. Another peak is graphite-like BC_3, the formation of BC_3 is substituting a carbon atom by B atom on edges or inside without damaging of the carbon skeletons. Therefore, this BC_3 doped type only improves the electronic conductivity of various NVP-C-B samples without accelerating the Na^+ diffusion across the carbon coated layer. As for the BC_2O and BCO_2, although the introduction of heteroatom O atom is not beneficial to increase the electronic conductivity of the carbon layer, this two doped types could remarkably create numerous extrinsic defects and active sites, which could allow rapid surface Na^+ absorption and ultrafast Na^+ diffusion in the carbon coated layer. Therefore, in various NVP-C-B samples, the NVP-C-B0.38% with the largest total amount of BC_2O + BCO_2 (66.6% for NVP-C-B0.24%, 79.8% for NVP-C-B0.38% and 65.2% for NVP-C-B0.51%), shows the best electrochemical performance, followed by NVP-C-B0.24% and NVP-C-B0.51%, and this also shows a high degree of consistency with the I_D/I_G ratio of Raman spectra (Fig. S4†).

However, it must be point out that the mechanism of B-doped carbon coating for the improvement of the electrochemical performance in SIBs and LIBs are different. In LIBs, due to the ionic radius of Li^+ is much smaller than Na^+, the Li^+ could freely

pass through the graphite-like amorphous carbon coated layer. But for SIBs, the graphite-like carbon coated layer has a strong resistance for Na^+ insertion/extraction.[37] Therefore, in LIBs, B-doped carbon coated electrode material with the largest amount of BC_3 or the minimize total content of BC_2O + BCO_2 exhibits the best electrochemical performance.[9] However, in SIBs, the NVP-C-B with the largest total amount of BC_2O + BCO_2 exhibits the best electrochemical performance. In orther word, the extrinsic defects caused by B-doping in the carbon coated layer could accelerate Na^+ diffusion, and as a result, the electrochemical performance is improved obviously. Fig. 7b shows a visual schematic illustration of Na^+ diffuse across the B-doped carbon coated layer in NVP-C-B sample. Based on the above analysis, the NVP-C-B0.38% with the largest diffusion velocity of Na^+ shows the best electrochemical performance in all NVP-C-B samples.

To explore the effects of B-doped carbon coating on electronic conductivity, the electronic conductivity measurement was carried out using a RTS-4 linear four-point probe measurement system. The values of NVP-C, NVP-C-B0.24%, NVP-C-B0.38% and NVP-C-B0.51% powders are 2×10^{-4}, 1.32×10^{-2}, 5.29×10^{-3} and 2.06×10^{-3}. Obviously, after B-doped into the carbon layer, the electronic conductivity of all NVP-C-B samples are higher than that of NVP-C, indicating B-doped carbon coating is conducive to increasing the electronic conductivity of $Na_3V_2(PO_4)_3$ composites.

Furthermore, to investigate the positive effect of boron doped carbon coating on kinetics of the electrode process, electrochemical impedance spectroscopy (EIS)

measurements of NVP-C and various NVP-C-B samples are performed. Fig. 8a shows the Nyquist plots and equivalent circuit of the various samples, which are collected in a 10 mV AC potential signal in the frequency range of 1 MHz to 10 mHz at full charge state (4.0 V) after four charge/discharge cycles. All curves include a semicircle in the high-frequency and a straight-line in the low frequency, indicating that the electrochemical process is controlled by both charge transfer and diffusion of sodium ion.[38] To further analyze impedance spectra, the EIS spectra are fitted with the equivalent circuit model, as shown in the inset of Fig. 8a. The R_s and CPE represent the electrolyte resistance, double layer capacitance and capacity of the surface layer, respectively. R_{ct} is the charge transfer resistance. The Warburg impedance (W_o) represents the diffusion behavior at low frequency.[22] The simulated data from the equivalent circuit model well fit the impedance data for both NVP-C and NVP-C-B samples. The EIS parameters of NVP-C and various NVP-C-B electrodes obtained from fitting are listed in Table 1. As it can be seen in Table 1, R_s of NVP-C is similar with various NVP-C-B samples; however, R_{ct} of NVP-C are much higher than those of NVP-C-B electrodes. Moreover, the NVP-C-B0.38% exhibits the lowest R_{ct} in three NVP-C-B samples. These results confirm that the B-doped carbon coating could effectively increase the electron conductivity of $Na_3V_2(PO_4)_3$ composites. Furthermore, the diffusion coefficient (D_{Na+}) of sodium ions can be calculated from the plots in the low frequency region, and the equation can be expressed as[39,40]

$$D = \frac{R^2 T^2}{2 A^2 n^4 F^4 C^2 \sigma^2} \tag{1}$$

19

$$Z_{re} = R_e + R_{ct} + \sigma\omega^{1/2} \tag{2}$$

where R is the gas constant, T is the absolute temperature, A is the surface area of the cathode, n is the number of electrons per molecule during oxidization, F is the Faraday constant, and C is the concentration of sodium ions (3.47×10^{-3} mol cm^{-3}), which can be calculated from the density and the molecular weight. σ is the Warburg factor which is related to Z_{re} (shown in equation (2)) and ρ and M are the density and the molecular weight of the materials, respectively. Fig. 8b displays the relationship between Z_{re} and the reciprocal square root of frequency ($\omega^{-1/2}$) in the low frequency region and the value of σ for NVP-C and various NVP-C-B are exhibited in Table 1. The calculated diffusion coefficients of the sodium ions (D_{Na+}) of NVP-C and various NVP-C-B are shown in Table 2. Notably, the D_{Na+} of various NVP-C-B are higher than that of NVP-C, indicating after B-doping in the carbon coated layer, numerous extrinsic defects and active sites are created, which could allow rapid surface Na$^+$ absorption and ultrafast Na$^+$ diffusion in the carbon coated layer. But more importantly, the NVP-C-B0.38% exhibits the largest D_{Na+} in all three NVP-C-B samples, suggesting that the most extrinsic defects are existed in NVP-C-B0.38%, and this also exhibits a high consistency with the I_D/I_G ratio of Raman spectra and XPS spectra of B1s.

Conclusions

In conclusion, we initially utilized a facile sol-gel method to prepare a B-doped carbon-coated Na$_3$V$_2$(PO$_4$)$_3$ cathode material for SIBs, and found that, after

modication by boron doping, four common B-doping species: B_4C, BC_3, BC_2O and

BCO_2 are normally obtained in the carbon layer. The mechanism of B-doped carbon

coating for the improvement of the electrochemical performance in SIBs and LIBs are

different. In SIBs, the more amount of BC_2O + BCO_2 existed, the better of

electrochemical performance obtained, in other word, the most of extrinsic defects are

existed in NVP-C-B, this NVP-C-B displays superior rate capacity and excellent cycle

stability when they are used as cathode material for sodium storage. The suitable

B-doped carbon coating not only increase the electronic conductivity of electrode

materials, but also create numerous extrinsic defects and active sites which allow

rapid surface Na^+ absorption and ultrafast Na^+ diffusion in the carbon layer. Therefore,

this work tell us, through the creation of a large number of defect sites on the carbon

coating layer can improve the electrochemical propeties of electrode materials of SIBs,

especially the rate performance.

Acknowledgements

Notes and references

1 S. P. Ong, V. L. Chevrier, G. Hautier, A. Jain, C. Moore, S. Kim, X. H. Ma, G. Ceder, *Energy Environ. Sci.*, 2011, **4**, 3680.

2 V. Palomares, P. Serras, I. Villaluenga, K. B. Hueso, J. C. Gonzalez, T. Rojo, *Energy Environ. Sci*., 2012, **5**, 5884.

3 Y. Uebou, T. Kiyabu, S. Okada, J.-I. Yamaki, The Reports of Institute of Advanced Material Study, Kyushu University, 2002.

4 K. Saravanan, C. W. Mason, A. Rudola, K. H. Wong, P. Balaya, *Adv. Energy Mater.,* 2013, **3**, 444.

5 M. Sathiya, K. Hemalatha, K. Ramesha, J. M. Tarascon, S. Prakash, *Chem. Mater*., 2012, **24**, 1846.

6 Z. Jian, L. Zhao, H. Pan, Y. Hu, H. Li, W. Chen, L. Chen, *Electrochem. Commun*., 2012, **14**, 86.

7 J. Kang, S. Baek, V. Mathew, J. Gim, J. Song, H. Park, E. Chae, A. K. Rai, J. Kim, *J. Mater. Chem*., 2012, **22**, 20857.

8 W. Shen, C. Wang, H. Liu, W. Yang, *Chem. Eur. J*., 2013, **19**, 14712.

9 C. Wang, Z. Guo, W. Shen, Q. Xu, H. Liu, Y. Wang, *Adv. Funct. Mater*., 2014, **24**, 5511.

10 Y. Xu, W. Shen, A. Zhang, H. Liu, Zi. Ma, *J. Mater. Chem. A*, 2014, **2**, 12982.

11 Y. H. Jung, C. H. Lim, D. K. Kim, *J. Mater. Chem. A*, 2013, **1**, 11350.

12 W. Song, X. Ji, Z. Wu, Y. Zhu, Y. Yang, J. Chen, M. Jing, F. Lia, C. E. Banks, *J. Mater. Chem. A*, 2014, **2**, 5358.

13 C. Zhu, K. Song, P. A. V. Aken, J. Maie, Y. Yu, *Nano Lett*., 2014, **14**, 2175.

14 G. Li, D. Jiang, H. Wang, X. Lan, H. Zhong, Y. Jiang, *Journal of Power Sources*, 2014, **265**, 325.

15 Z. Jian, W. Han, X. Lu, H. Yang, Y.-S. Hu, J. Zhou, Z. Zhou, J. Li, W. Chen, D. Chen, L. Chen, *Adv. Energy Mater*., 2013, **3**, 156.

16 C. Wang, H. Liu, W. Yang, *J. Mater. Chem*., 2012, **22**, 5281.

17 H. Li, H. Zhou, *Chem. Commun*., 2012, **48**, 1201.

18 C. H. Choi, M. W. Chung, H. C. Kwon, S. H. Parka, S. I. Woo, *J. Mater. Chem. A*, 2013, **1**, 3694.

19 L. Zhao, Y.-S. Hu, H. Li, Z. X. Wang, L. Q. Chen, *Adv. Mater*., 2011, **23**, 1385.

20 H. Li, L. Shen, X. Zhang, J. Wang, P. Nie, Q. Che, B. Ding, *Journal of Power Sources*, 2013, **221**, 122.

21 C. Wang, Z. Y. Guo, W. Shen, A. Zhang, Q. Xu, H. Liu, Y. Wang, *J. Mater. Chem. A*, 2015, **3**, 6064.

22 W. Shen , C. Wang , Q. Xu , H. Liu, Y. Wang, *Adv. Energy Mater*., 2015, **5**, 201400982

23 Z.-S. Wu, W. C. Ren, L. Xu, F. Li, H.-M. Cheng, *ACS Nano*, 2011, **5**, 5463.

24 M. Wu, Y. Ren, N. Guo, S. Li, X. Sun, M. Tan, D. Wang, J. Zheng, N. Tsubaki, *Mater. Lett*., 2012, **82**, 124.

25 W. Duan, Z. Zhu, H. Li, Z. Hu, K. Zhang, F. Cheng, J. Chen, *J. Mater. Chem. A*, 2014, **2**, 8668.

26 Z. Jian, C. Yuan, W. Han, X. Lu, L. Gu, X. Xi, Y.-S. Hu, H. Li, W. Chen, D. Chen, Y. Ikuhara, L. Chen, *Adv. Funct. Mater*., 2014, **24**, 4265.

27 H. Li, Y. Bai, F. Wu, Y. Li, C. Wu, *Journal of Power Sources*, 2015, **273**, 784.

28 H. Li, L. Shen, K. Yin, J. Ji, J. Wang, X. Wang, X. Zhang, *J. Mater. Chem. A*, 2013, **1**, 7270.

29 C. Wang, W. Shen, H. Liu, *New J. Chem.*, 2014, **38**, 430.

30 J. Liu, K. Tang, K. P. Song, P. A. van Aken, Y. Yu, J. Maier, *Nanoscale*, 2014, **6**, 5081.

31 H. Wang, T. Maiyalagan, X. Wang, *ACS Catal.*, 2012, **2**, 78.

32 S. Wang, E. Iyyamperumal, A. Roy, Y. Xue, D. Yu, L. Dai, *Angew. Chem. Int. Ed.*, 2011, **50**, 11756.

33 Y. Tang, L. Yin, Y. Yang, X. Bo, Y. Cao, H. Wang, W. Zhang, I. Bello, S. T. Lee, H. Cheng, C. S. Lee, *ACS Nano*, 2013, **6**, 1970.

34 G. Jo, S. Shanmugam, *Electrochem. Commun.*, 2012, **25**, 101.

35 J. Ozaki, N. Kimura, T. Anahara, A. Oya, *Carbon*, 2007, **45**, 1847.

36 T. Wu, H. Shen, L. Sun, B. Cheng, B. Liu, J. Shen, *New J. Chem.*, 2012, **36**, 1385.

37 Y. Cao, L. Xiao, M. L. Sushko, W. Wang, B. Schwenzer, J. Xiao, Z. Nie, L. V. Saraf, Z. Yang, J. Liu, *Nano Lett.*, 2012, **12**, 3783.

38 Z. Hu, K. Zhang, H. Gao, W. Duan, F. Cheng, J. Liang, J. Chen, *J. Mater. Chem. A*, 2013, **1**, 12650.

39 H. Liu, Q. Cao, L. Fu, C. Li, Y. Wu, H. Wu, *Electrochem. Commun.*, 2006, **8**, 1553.

40 H. Liu, C. Li, H. Zhang, L. Fu, Y. Wu, H. Wu, *J. Power Sources*, 2006, **159**, 717.

Scheme 1. Crystal structure of NASICON-type Na$_3$V$_2$(PO$_4$)$_3$, 3D framework of a) ~ b) Na1site and c) ~ d) Na2 site.
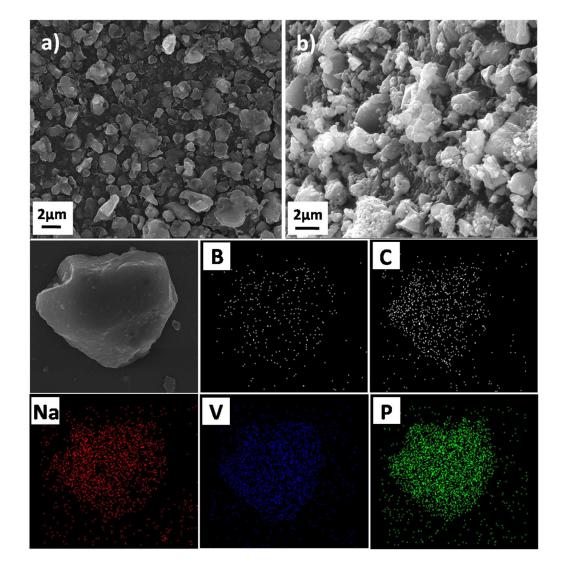
Fig. 1 SEM images of a) NVP-C and b) NVP-C-B0.38% samples, and the EDX mapping images of the NVP-C-B0.38% sample.
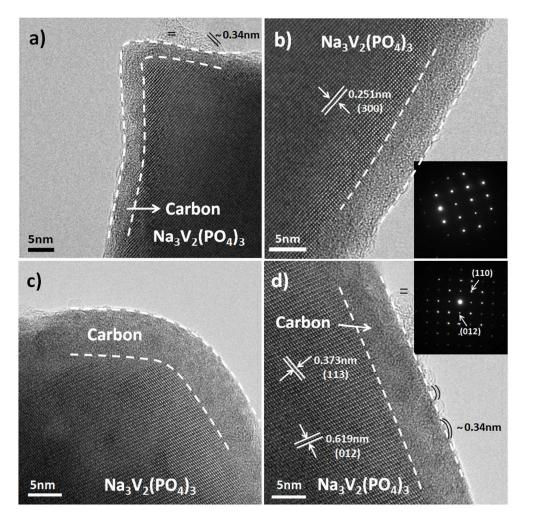
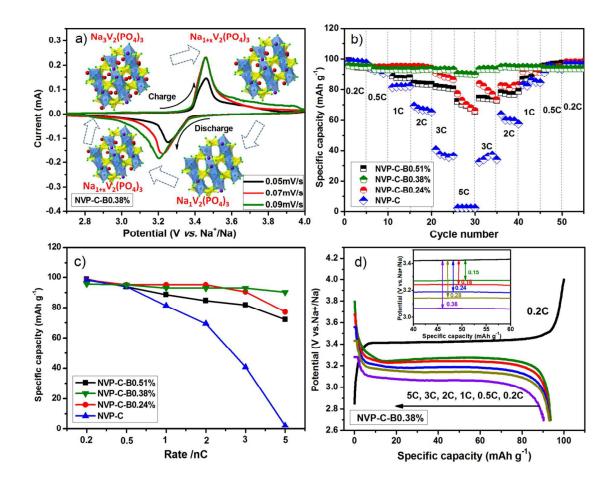**Fig. 2** HRTEM images of a) and b) NVP-C, c) and d) NVP-C-B0.38% samples.

Fig. 3 The electrochemical performances of as-fabricated NVP-C and various NVP-C-B electrode materials, a) cyclic voltammograms (CV) curves at various scan rates, b) the discharge capacities obtained at various C-rates, c) comparison of the rate capability, d) the potential profiles of NVP-C-B0.38% at various C-rates. All the tests were performed in the potential window of 2.7~4.0 V (*vs.* Na$^+$/Na).

Fig. 4 The electrochemical performances of as-fabricated NVP-C and various

NVP-C-B electrode materials, cycle performances at a) 0.2 C, b) 1C and c) 5 C, d)

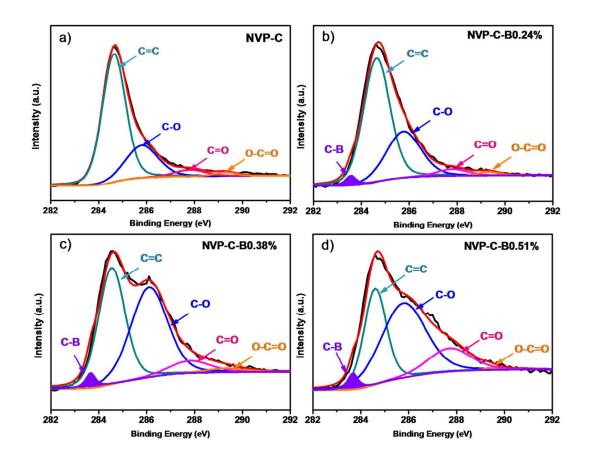coulombic efficiency and cycle performance at 10 C.

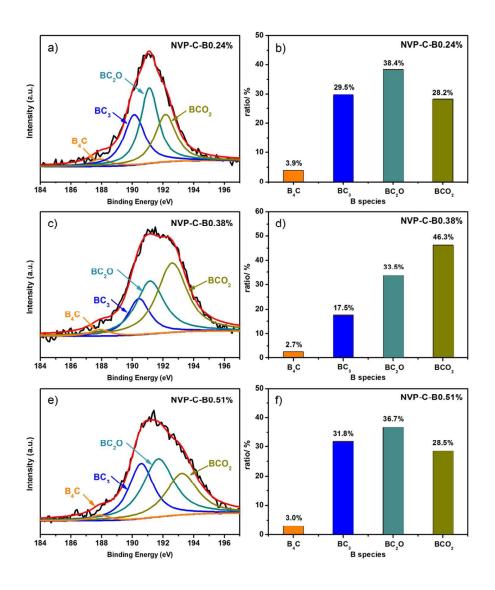**Fig.5** a-d) High-resolution XPS spectra of C1s for the NVP-C and various NVP-C-B samples.

Fig. 6 High-resolution XPS spectra of B1s for the a) NVP-C-B0.24%, c) NVP-C-B0.38%, e) NVP-C-B0.51% and b), d), f) corresponding the histogram for ratio of different B species in various NVP-C-B samples.
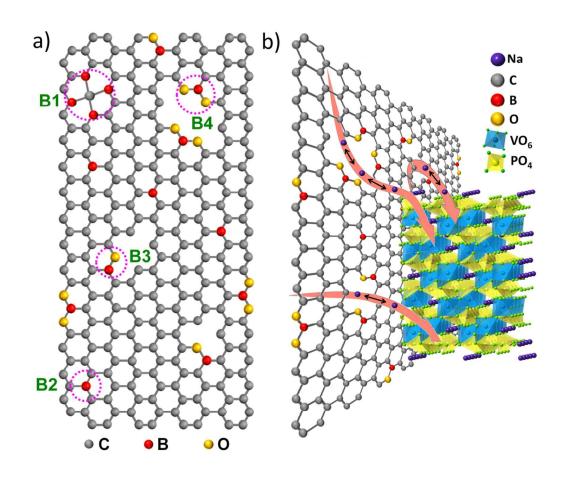
Fig. 7 a) Schematic structure of the bonding conditions of B in a carbon lattice, B1:B_4C, B2:BC_3, B3:BC_2O and B4:BCO_2; b) a schematic illustration of sodium ion storage mechanism in the NVP-C-B composite electrode.
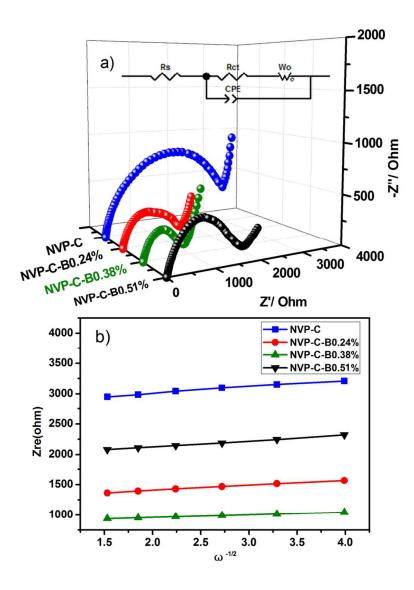
Fig. 8 a) Nyquist plots of NVP-C sample and various NVP-C-B samples at a stage of charge (4.0 V), b) the relationship between Zre and $\omega^{1/2}$ in the low frequency region.

Table 1. EIS parameters for NVP-C and various NVP-C-B samples obtained from

equivalent circuit of EIS results.

Entry [a]	NVP-C	NVP-C-B0.24%	NVP-C-B0.38%	NVP-C-B0.51%
R_s /ohm	9.275	5.951	6.662	6.248
R_{ct}/ohn	2554	1095	784	1504
CPE/F	2.141E-5	1.628E-5	2.11E-5	1.302E-5
W_o/S s$^{-0.5}$	0.003002	0.005409	0.01155	0.008226
σ/ohm cm^2 s$^{-0.5}$ [b]	106.3	82.7	42.7	96.5

[a]The EIS measurements of all samples are all carried out in the frequency range of
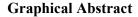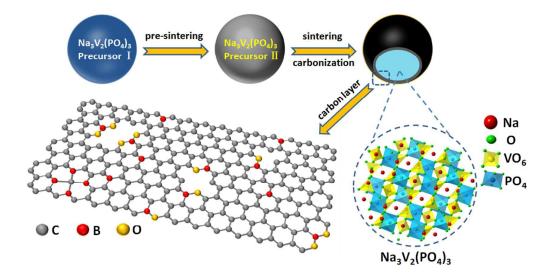
1MHz to 10mHz at the charge state (4.0V).

[b] σ, the slope of the Zre versus $\omega^{-1/2}$ plot.

Table 2. The calculated diffusion coefficients of the sodium ions (D_{Na+}) of NVP-C

and various NVP-C-B samples.

Samples	NVP-C	NVP-C-B0.24%	NVP-C-B0.38%	NVP-C-B0.51%
D_{Na+} (cm^2/s)	4.0×10^{-14}	6.63×10^{-14}	2.48×10^{-13}	4.92×10^{-14}

Graphical Abstract

Boron-doped carbon coated $Na_3V_2(PO_4)_3$ is prepared, and different impacts of various carbon-boron species on the improvement of electrochemical performance for sodium and lithium ion batteries are analyzed and discussed in this work.